GEOMATICS AND ENVIRONMENTAL ENGINEERING • Volume 19 • Number 2 • 2025

https://doi.org/10.7494/geom.2025.19.2.71

Davide Morale[1], Claudio Parente[2], Salvatore Falanga Bolognesi[3]

Comparison of Machine-Learning Algorithms for SPOT 7 Multispectral Image Classification

Abstract: Precise and timely land-cover identification plays an important role in effective environmental monitoring and land management. This study compares the performance of five machine-learning classifiers – support vector machine (SVM), decision tree (DT), normal Bayes (NB), random forest (RF), and *k*-nearest neighbor (k-NN) – in the land-cover mapping of the Agro Nocerino Sarnese area (Southern Italy) using high-resolution SPOT 7 pan-sharpened multispectral images with a pixel size of 1.5 m × 1.5 m. The data set consisted of blue, green, red, and near-infrared (NIR) bands and was processed with Orfeo ToolBox (OTB) software. Two data sets were analyzed: DS-3B (which included only the visible bands [blue, green, and red]), and DS-4B (which also included the NIR band). A comparison of the classifiers' performances across various land-cover classes was conducted in order to assess their respective classification accuracy. The results showed that SVM and k-NN achieved the highest overall accuracy levels (93% and 92%, respectively) using only the visible bands, whereas the decision tree classifier performed best when the NIR band was included. Random forest achieved excellent accuracy in vegetation classes (88–99%) but struggled with misclassifications in bare soil and man-made classes such as buildings and roads. These results emphasized the significant impact of data set characteristics on classifier performance as well as the importance of band selection and pan-sharpening techniques in high-resolution land-cover mapping.

Keywords: land-cover classification, machine learning, SPOT 7, Orfeo ToolBox, support vector machine, random forest, decision tree, high-resolution imagery

Received: December 30, 2024; accepted: March 19, 2025

1 International PhD Programme "Environment, Resources, and Sustainable Development," University of Naples "Parthenope," Department of Science and Technology, Naples, Italy, email: davide.morale001@studenti.uniparthenope.it; Fondazione CMCC-Centro Euro Mediterraneo sui Cambiamenti Climatici, Italy, email: davide.morale@cmcc.it, https://orcid.org/0000-0001-8139-8935

2 University of Naples "Parthenope," Department of Science and Technology, Naples, Italy, email: claudio.parente@uniparthenope.it (corresponding author), https://orcid.org/0000-0002-8328-9764

3 Ariespace s.r.l., Naples, Italy, email: salvatore.falanga@ariespace.com, https://orcid.org/0000-0003-0134-2574

1. Introduction

Remote sensing allows for the acquisition of qualitative and quantitative information from an object, area, or phenomenon through the analysis of data that is acquired from a remote device; i.e., a sensor that is placed onboard a satellite that is not in direct contact with an object, area, or phenomenon that is being investigated [1]. The classification of high-resolution satellite images is a topic of fundamental importance for identifying the various land-cover areas on the Earth's surface; this is useful for monitoring cultivated fields in agriculture as well as environmental or hydrological resources [2]. To obtain information on land cover, a classification of remotely sensed data is carried out; areas or pixels with similar spectral characteristics are assigned to classes or categories – each representing a different type of land-cover feature.

To effectively monitor and analyze land cover, various remote-sensing tools and data sets are employed – each offering unique strengths and limitations depending on the spatial resolution, coverage, and temporal dynamics. The CORINE land-cover data set (CLC) provides a broad land-cover classification for Europe at a 100-meter resolution [3]; it is suitable for large-scale mapping, but it has limitations in capturing fine-scale details – particularly in mixed urban-natural areas [4]. ESA's Dynamic World data set offers global land-cover data at 10- to 30-meter resolutions with real-time updates [5]; however, its accuracy can be influenced by seasonal variability and topographical factors [6].

Among the various land-cover products that are provided by international agencies, there is a significant lack of data sets that have been derived from high-resolution imagery. While existing data sets offer valuable information at coarser spatial resolutions, they often fail to capture the fine-scale variations in land cover that are essential for accurate environmental monitoring and decision-making [7]. High-resolution remote-sensing data could greatly enhance the precision of land-cover classification and provide more-detailed insights into local-scale changes that are often obscured in lower-resolution data sets.

Working with high-resolution or very-high-resolution (VHR) images (which feature sub-meter level detail) presents heightened challenges for classification tasks; these difficulties are due to the desired high-resolution output and the level of uncertainty in the predictions [8]. Therefore, the choice of an algorithm to use is essential for identifying land use-land cover (LULC) [9] and the separation thresholds (in terms of the spectral response) between the various classes. Machine learning (ML) offers the potential for the effective and efficient classification of remotely sensed imagery, enables the handling of high-dimensional data, and provides the ability to map classes with very complex characteristics [10].

Currently, ML is constantly evolving; it uses designed calculation algorithms to emulate human intelligence without explicit programming [11], which allows it to develop practical software for computer vision [12], self-driving cars [13], and other applications within the science and engineering fields (this also includes geoscience [14] and remote sensing [10]). ML is a subset of artificial intelligence that enables computers to learn from data and experiences without being explicitly programmed; however, the classification methods can be divided into supervised and unsupervised learning.

Supervised learning is based on providing a computer system with training and test sets of labeled data, which allow for the building of a model that is capable of identifying unlabeled data [15]. With this model, the analyst acts as a guide and teaches the algorithm which results to generate. In supervised ML, the algorithm learns from a data set that has been previously labeled and provides a predefined output. In this case, the identification of sample areas (training sites) that are related to a specific land-cover area for training algorithms is essential for classifying satellite images with supervised ML. The algorithms that fall within supervised machine learning are several [16]; among others, these include support vector machine (SVM) [17], neural nets [18], logistic regression [19], normal Bayes (NB) [20], random forest (RF) [21], decision tree (DT) [22], and *k*-nearest neighbor (k-NN) [23].

However, when the data is all unlabeled (there are no training sites), then the learning process is labeled "unsupervised." In other terms, information that is neither classified nor labeled allows an algorithm to classify data autonomously. The purpose of algorithms is to group unsorted information according to its similarities, patterns, and differences without any prior training with the data [24]. The most-used algorithms in unsupervised machine learning are hierarchical clustering [25], *k*-means [26] and isodata [27]. The aim of this study is to perform land-cover classification using high-spatial-resolution (1.5 m) SPOT 7 imagery and ML algorithms. The SPOT 7 satellite enables detailed land-cover classifications – particularly in complex areas.

The classifications were carried out using supervised ML algorithms, including SVM, DT, NB, RF, and k-NN. Through the comparison of ML-based classification techniques, our research provides a novel contribution by examining a unique area that is characterized by complex urban-rural landscapes. Such landscapes present challenges that have yet to be fully addressed in the literature, making these regions particularly suitable for testing and refining classification methods in such complex environments. The applications were carried out using Quantum GIS (QGIS) software (ver. 3.28) and Orfeo ToolBox (OTB). The paper is structured in the following way: in Section 2, the study area and satellite data are presented, as are as the applied methods; in Section 3, the results are reported and discussed; and in Section 4, our conclusions are stated.

2. Data and Methods

2.1. Study Area and Data Set

The study area that was selected for this article is a portion of the municipality of Sarno, which is located in the province of Salerno in Campania (Italy); it covers an area of 6 km × 4 km (Fig. 1).

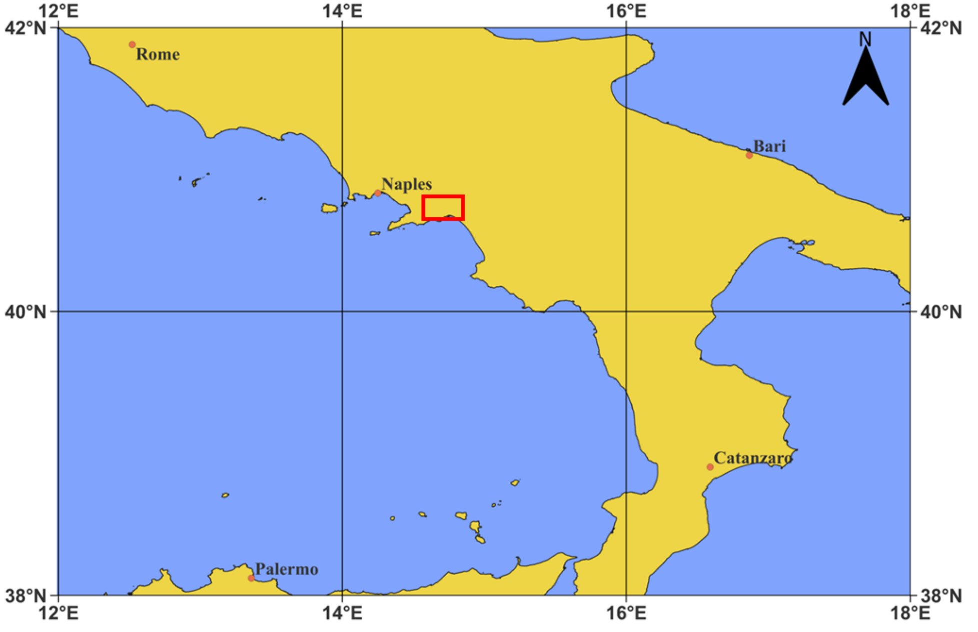

Fig. 1. Geolocalization of Sarno (red rectangle) in equirectangular projection and WGS 84 ellipsoidal coordinates

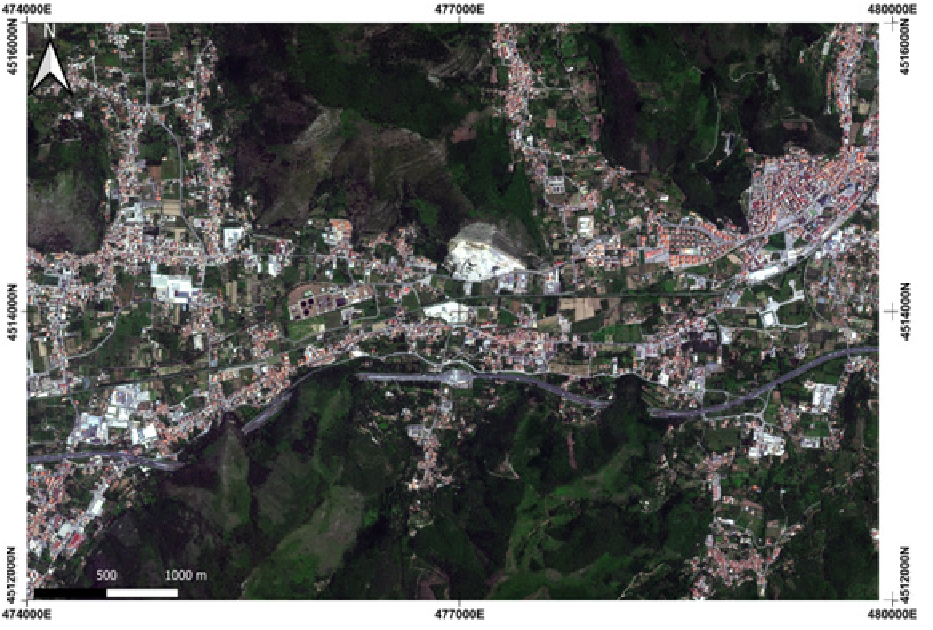

Fig. 2. True-color RGB composite of SPOT 7 imagery that was acquired on June 7, 2019, at UTM-WGS 84 plane coordinates

Geographically, Sarno is part of the Agro Nocerino Sarnese (the southern part of the Campanian Plain); it develops on the slopes of Mount Saro and the banks of the Sarno River. Sarno's economy is essentially based on agricultural production and canning; therefore, the territory is characterized by extensive vegetation and many agricultural and food infrastructures. In terms of land cover, the Sarno area is primary characterized by crops (herbaceous and tree), forest vegetation, buildings, and greenhouses. The study area extends to the following UTM-WGS84 (Zone 33 N) plane coordinates: E_1 = 474,000 m; E_2 = 480,000 m; N_1 = 4,512,000 m; and N_2 = 4,516,000 m. Figure 2 shows the true-color RGB composite of the SPOT 7 imagery that was used for this study.

SPOT 7 (Satellite pour l'Observation de la Terre) was launched on June 1, 2014, and ceased operations on March 17, 2023. SPOT 7 was designed to provide high-resolution wide-area optical imagery to support the knowledge and management of Earth's resources, detect and forecast the phenomena that involved climatology and oceanography, and monitor human activities and natural phenomena [28].

The SPOT 7 data set offered several key advantages, including its high geometric resolution and the availability of both panchromatic and multispectral bands, thus enabling the application of pan-sharpening techniques. Additionally, the data set's high temporal resolution (with scene-acquisition intervals that ranged from one to three days) facilitated the capture of images with minimal cloud cover, thus enhancing the data quality and reliability. However, its high-resolution images typically covered smaller spatial extents as compared to its medium-resolution images; with a geometric resolution of 30 m, for instance, the swath of a Landsat 9 image spans 185 km [29]. This is significantly larger than the 60 km swath of a SPOT 7 image [28].

The SPOT 7 data set was comprised of four multispectral bands (blue, green, red, and near infrared) with a resolution of 6 m and one panchromatic (PAN) band with a resolution of 1.5 m [28] (as reported in Table 1). The satellite imagery was pansharpened in order to achieve the same geometrical resolution in the multispectral bands as could be found in the panchromatic band [30, 31]; it was also orthorectified. Thanks to the pan-sharpening technique, all of the multispectral band data had a geometric resolution that was equal to 1.5 m.

Table 1. Main characteristics of SPOT 7 images

Band	Wavelength [μm]	Resolution [m]
Band 1 – Blue	0.45–0.52	6.0
Band 2 – Green	0.53–0.59	6.0
Band 3 – Red	0.62–0.69	6.0
Band 4 – Near Infrared	0.76–0.89	6.0
PAN	0.45–0.75	1.5

2.2. Classification Methods

The classification of satellite images is a crucial process in remote sensing; this enables the extraction of valuable information from Earth observation data. The following workflow (Fig. 3) outlines the steps that are necessary for classifying satellite imagery.

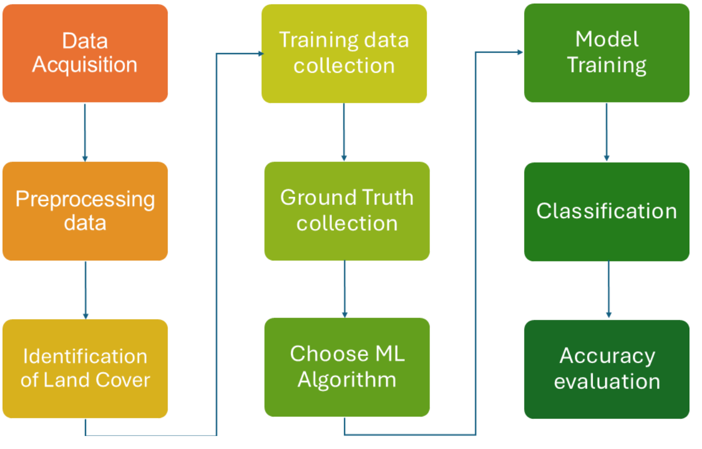

Fig. 3. Workflow of adopted approach for satellite image classification – detailing steps from data acquisition through accuracy evaluation

The first step of the application is to identify the land cover through a visual investigation in order to determine the main classes of a study area. The following classes were considered in this work: buildings, roads, bare soil, greenhouses, and herbaceous and tree crops.

During the training phase of each ML algorithm, it was necessary to identify training sites to statistically characterize the reflectance of each class that was considered; this enabled a signature analysis to represent the variations in the reflectance or emittance of a material across wavelengths [32]. After determining a statistical characterization for all classes, the classification was conducted by evaluating the reflectance of each pixel and choosing which signature had the most resemblance to it.

The experiments were carried out considering two data sets: DS-3B (which included the red, green, and blue bands), and DS-4B (which included all of the multispectral bands (visible + NIR).

Machine-Learning Algorithms

In this part, we introduce and discuss machine learning classifiers used in this work: support vector machine (SVM), decision tree (DT), normal Bayes (NB), random forest (RF), and *k*-nearest neighbors (k-NN). For each algorithm, we will explore its underlying principles, strengths, and typical applications in the context of the classification tasks addressed in this study.

Support Vector Machine. SVMs represent a powerful classification model in machine learning that is based on statistical learning theory [33]; this is a supervised non-parametric technique that does not assume an underlying data distribution. The method relies on a labeled data set, and the SVM training algorithm aims to find a hyperplane that separates the data set into a predefined number of classes that are in alignment with the training examples [34, 35]. The separating hyperplane defines a decision boundary that minimizes classification errors during the training [36]; therefore, the algorithm identifies the optimal separating hyperplane that maximizes the margin – the distance between the hyperplane and the support vectors [37]. Mathematically, this can be expressed as finding the hyperplane that is defined by Equation (1) given a specific data set $[(x_1, y_1), (x_2, y_2), ..., (x_n, y_n)]$, where x_i represents the feature vector, and y_i represents the corresponding class label:

$$y(i) = w^T x + b = 0 \tag{1}$$

where w is a vector that is normal to the hyperplane, and b is the bias term. The margin is defined as the distance between the support vectors and the hyperplane. The SVM algorithm maximizes this distance by solving the following optimization problem:

$$\min \frac{1}{2} \|w\|^2 \tag{2}$$

which is subject to the following constraints:

$$y_i (w^T x_i + b) \geq 1, \quad \forall_i = 1, 2, \ldots, n \tag{3}$$

This optimization seeks the values of w and b that maximize the margin while ensuring that all data points are correctly classified. In other words, each point must lie on the correct side of the margin boundary.

In a 2017 study that was conducted by Wang et al. [38], the influence of the parameters that define the support vector machine algorithm was evaluated by comparing its results with those of other methods. Similarly, the studies by Foody and Pal [39, 40] proposed a method that was based on the SVM algorithm for the multi-class classification of aerial sensors and Landsat ETM+ data, focusing on the impact of the training set size on the classification accuracy.

Decision Tree. DT is a non-parametric supervised-learning algorithm that is used for both classification and regression tasks. This algorithm relies on sequential tests and decisions to perform its classifications. It has a tree-like structure, with a root node, branches (which represent decision paths), nodes (where tests are applied), and leaves (which represent class labels) [41]. The process of dividing a node into two or more sub-nodes is known as the splitting phase [42]. At each node, the Gini impurity is calculated; this represents the probability that a randomly chosen sample is incorrectly labeled at a specific node [43]. This index is given by the following equation:

$$Gini(j) = 1 - \sum_{i=1}^{n} p_i^2 \tag{4}$$

where p_i is the proportion of the samples that belong to class i in node j.

In 2001, Pal and Mather [44] obtained excellent results in terms of accuracy by applying the decision tree algorithm for land-use classification; specifically, they used Landsat 7 ETM+ satellite images of an agricultural area near Littleport (UK). Berhane et al. [45] applied DT to classify wetlands in the Selenga River Delta (Lake Baikal, Russia) using high-resolution WorldView-2 satellite images. Finally, Friedl and Brodley's study [46] examined various decision tree algorithms for land-cover classifications based on three distinct remote-sensing data sets. The research emphasized that decision trees provided key advantages for remote-sensing applications thanks to their straightforward intuitive structure, their nonparametric nature, and their ability to handle nonlinear and noisy relationships between input features and class labels.

Normal Bayes. NB is a probabilistic machine-learning algorithm that relies on assumptions about the statistical distribution of the classes to be investigated. This algorithm uses training sites to estimate the mean and variance of each class; these are then used to evaluate the probability of assigning a pixel to a specific class [47–49]. A normal Bayes classification is based on Bayes' theorem:

$$P(C \mid X) = \frac{P(X \mid C)\,P(C)}{P(X)} \tag{5}$$

where $P(C \mid X)$ is the posterior probability of class C given feature X, $P(X \mid C)$ is the likelihood of observing X given class C, $P(C)$ is the prior probability of class C, and $P(X)$ is the evidence or total probability of observing X. Under the naïve assumption that features are independent, the likelihood $P(X \mid C)$ becomes the product of the individual feature probabilities:

$$P(X \mid C) = \prod_{i=1}^{n} P(x_i \mid C) \tag{6}$$

where x_i is the value of feature i for observation X. For each class C_k, the algorithm calculates the mean and variance for each feature x_i using the training data.

The prior probability $P(C_k)$ is calculated based on the frequency of each class in the training data:

$$P(C_k) = \frac{T_k}{T} \tag{7}$$

where T_k is the number of training samples in class C_k, and T is the total number of training samples.

To classify a new observation X, the algorithm calculates the posterior probability $P(C_k | X)$ for each class C_k. Assuming a Gaussian distribution for the feature values, the likelihood $P(x_i | C_k)$ is given by the following:

$$P(x_i | C_k) = \frac{1}{\sqrt{2\pi\sigma_{i,k}^2}} \exp\left(-\frac{(x_i - \mu_{i,k})^2}{2\sigma_{i,k}^2} \right) \tag{8}$$

The class with the highest posterior probability is selected as the predicted class for a pixel or region.

In Solares and Sanz [50], various Bayesian network algorithms (including normal Bayes) were compared in terms of their thematic accuracy for classifying multispectral and hyperspectral remote-sensing images. In a study by Yang and Yu [51], this algorithm was applied for the texture classification of high-resolution satellite images (specifically, GeoEye-1 imagery), with the aims of achieving automation and optimal accuracy.

Random Forest. RF is a widely used ensemble-learning algorithm that builds its models based on the results from different decision trees; its final prediction result is obtained by averaging the outputs or by majority voting [52]. This algorithm is based on a combination of decision trees that make up a so-called "forest"; therefore, a specific number of decision trees are trained using a random sample of an entire data set for each tree [53]. The final classification decision is made through majority voting or by averaging class-assignment probabilities that have been calculated from all of the trees that have been produced. Unlabeled data is evaluated against all of the decision trees that have been created in the "forest," and each tree votes for class membership; the class membership with the most votes will be the one that is ultimately selected [54].

Specifically, the random forest algorithm has been employed to classify agricultural crops using multitemporal SAR images [55], forests in the Anderson River area (Fort St. James, British Columbia, Canada) using remote-sensing and geographic data [56], and urban areas using Ikonos and QuickBird satellite images (which featured four multispectral bands) [57].

***k*-Nearest Neighbor.** The k-NN algorithm is a non-parametric method [58] that uses training sites and classifies objects by considering the closest training sites (*k*) in a feature space [59]; i.e., it classifies unlabeled pixels by considering their similarities to training set examples. This algorithm considers each pixel of a data set as a point in *n*-dimensional space and classifies it based on its distance from the samples of the training set; the most commonly used distances are the Euclidean and Manhattan distances [60]. Once the distance between the unclassified pixel and all of the training data points is calculated, the next step is to select the k-NN. The classification decision is then made based on a by majority vote; the algorithm counts the class labels of the k-NN, and the most frequently occurring class is assigned to the unclassified pixel. However, the computational efficiency of the k-NN algorithm is not optimal, as it struggles to handle large data sets; this is due to two main issues: memory consumption, and computational cost [61]. The k-NN algorithm was applied by Thanh Noi and Kappas [62] for land use/land cover classification in the Red River Delta of Vietnam using Sentinel-2 data; it achieved excellent thematic accuracy as the number of training sites increased. In a study by Abedi and Bonyad [63], this algorithm was used to integrate IRS-P6 LISS III satellite-imagery data with ground-inventory data for forest-attribute estimation and mapping, thus demonstrating the effectiveness of k-NN in terms of overall accuracy and the kappa coefficient.

2.3. Accuracy Assessment

Test sites are used to evaluate the thematic accuracy of sets of results. These sites act as representative samples for the classes that are under consideration, ensuring that they are adequately and significantly represented [64].

To describe the accuracy of the thematic map that is obtained from the classification process, we refer to the confusion matrix [65]. This matrix uses test sites or ground-truth data as a reference. To evaluate the classification accuracy, the following metrics are calculated: producer accuracy (PA), user accuracy (UA), omission error (OE), commission error (CE), overall accuracy (OA), and F1-score.

PA represents the probability of correctly classifying a specific feature within a particular area (as defined by Fung and LeDrew [66]). For a particular class *j*, PA is calculated as follows:

$$PA_j = \frac{VA_j}{PB_j} \tag{9}$$

where VA_j is the number of pixels that are correctly classified as class *j*, and PB_j represents the total number of pixels that belong to this class in a reference image.

On the other hand, UA indicates the likelihood that a region that is classified under a specific category in a thematic map truly belongs to this category; it is calculated as the ratio of the correctly classified pixels for a given class to the total number of pixels that were assigned to that class in a map. For class *j*, UA is expressed as follows:

$$UA_j = \frac{VA_j}{PD_j} \tag{10}$$

where VA_j refers to the number of pixels that are correctly classified as class *j*, and PD_j is the total number of pixels that are assigned to class *j* in a thematic map.

OEs occur when pixels that belong to a reference class are excluded from this class in a thematic map. This is inversely related to PA and can be calculated by using the following:

$$OE = 1 - PA \tag{11}$$

CEs arise when pixels are incorrectly included in a specific class in a thematic map; this is inversely related to UA and is given by the following:

$$CE = 1 - UA \tag{12}$$

OA reflects the percentage of pixels that are correctly classified across an entire test data set; this is determined as the ratio of the total number of correctly classified pixels to the total number of pixels in the data set. OA is computed by using the following equation:

$$OA = \frac{VA_j + VA_i + \ldots + VA_n}{P} \tag{13}$$

where VA_j, VA_i, ...,VA_n represent the number of correctly classified pixels for each class, and P denotes the total number of test pixels.

F1-score is a performance metric that balances the trade-off between omission and commission errors by combining PA and UA into a single value; it is calculated as the harmonic mean of PA and UA for a given class *j*:

$$F1_j = 2 \cdot \frac{PA_j \cdot UA_j}{PA_j + UA_j} \tag{14}$$

In the following subsections, the main characteristics of the ML algorithms that were used in our experiments and the available in OTB software that can be accessed in the QGIS environment are described.

3. Results and Discussion

The different classification performances of various ML algorithms were tested using OA, UA, PA, CE, OE, and F1-score. Tables 2 and 3 present the classification results for the DS-3B data set.

Table 2. UA and PA results that were achieved by applying ML algorithms to DS-3B data set (highest value[s] for each class highlighted in bold)

Methods	Classes											
	Buildings		Roads		Bare Soil		Tree Crops		Herbaceous Crops		Greenhouses	
	UA	PA	UA	PA	UA	PA	UA	PA	UA	PA	UA	PA
SVM	**0.98**	**0.89**	**0.92**	**0.96**	0.88	**0.96**	0.92	**0.92**	**0.91**	**0.91**	**0.99**	0.93
DT	0.90	0.84	0.84	0.90	0.83	0.85	0.93	0.89	0.86	0.93	**0.99**	0.94
NB	0.82	0.92	0.72	0.91	**0.91**	0.87	**0.99**	0.61	0.69	0.53	0.69	0.97
RF	0.44	0.62	0.79	0.39	0.28	0.31	0.93	0.89	0.85	0.92	**0.99**	**0.99**
k-NN	**0.98**	0.86	0.91	0.93	0.83	0.95	0.93	0.89	0.86	0.92	**0.99**	0.92

Table 3. CE and OE that occurred by applying ML algorithms to DS-3B data set

Methods	Classes											
	Buildings		Roads		Bare Soil		Tree Crops		Herbaceous Crops		Greenhouses	
	CE	OE	CE	OE	CE	OE	CE	OE	CE	OE	CE	OE
SVM	0.02	0.11	0.08	0.04	0.12	0.04	0.08	0.08	0.09	0.09	0.01	0.07
DT	0.10	0.16	0.16	0.10	0.17	0.15	0.07	0.11	0.14	0.07	0.01	0.06
NB	0.18	0.08	0.28	0.09	0.09	0.13	0.01	0.39	0.31	0.47	0.31	0.03
RF	0.56	0.38	0.21	0.61	0.72	0.69	0.07	0.11	0.15	0.08	0.01	0.01
k-NN	0.02	0.14	0.09	0.07	0.17	0.05	0.07	0.11	0.14	0.08	0.01	0.08

Figures 4 and 5 illustrate the OA, and F1-score values that were associated with the classifications of the DS-3B data set using the different machine-learning algorithms.

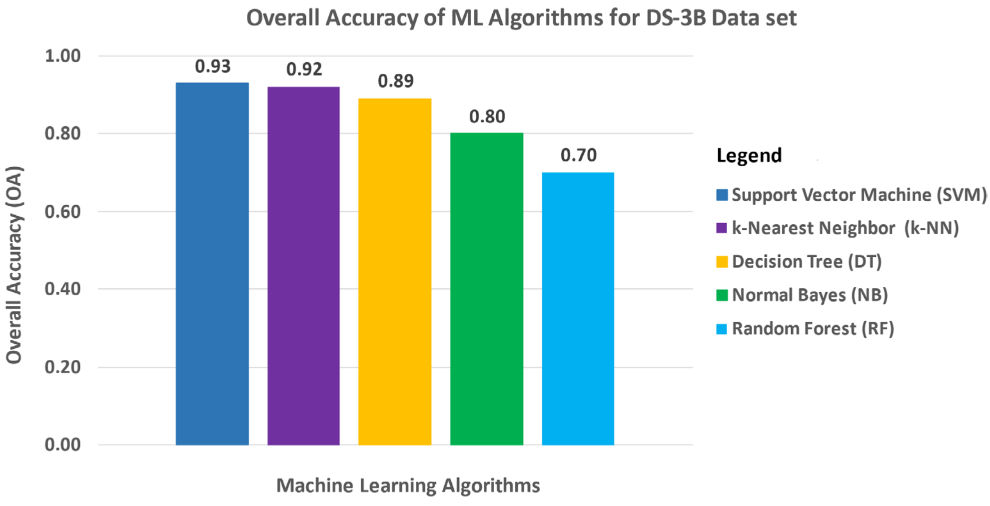

Fig. 4. OA levels that were achieved by different ML algorithms (SVM, k-NN, DT, NB, and RF) for DS-3B data set (colors represent respective algorithms as are indicated in legend)

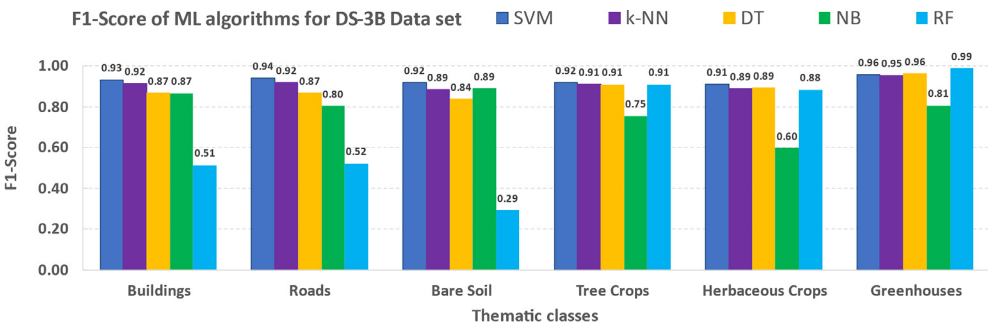

Fig. 5. F1-scores that were achieved by different ML algorithms (SVM, k-NN, DT, NB, and RF) for DS-3B data set (colors represent respective algorithms as are indicated in legend)

The best-performing algorithms were SVM and k-NN, with OA values of 93% and 92%, respectively. The third-best-performing algorithm was DT, with an OA value of 89%, followed by normal Bayes (NB) and RF, with the latter former obtaining the worst OA value (70%).

From the performance of RF, the most notable observations were its high accuracy for the vegetation classes (0.88–0.99) and its poor classifications for artificial surfaces such as roads, buildings, and bare soil (Fig. 5); the reason behind this inconsistency was its use of ensemble decision trees that had a bias toward class separability within a data set with high spectral variability between the classes. Within this study, vegetation resulted in a better spectral response than artificial surfaces did, leading RF to give vegetation a higher priority than the man-made class categories. RF's tendency toward overfitting the dominant spectral features may have also reduced its ability for classification generalization for mixed land cover.

Figure 6 shows a zoomed-in location within the study area; this displays the classification results and highlights the differences among the various ML methods (as are shown in Figure 7).

Tables 4 and 5 illustrate the classification results for the DS-4B data set. The top-performing model was DT (with 90% OA). The drop in performance for SVM and k-NN when using the DS-4B data set could have been linked to the pan-sharpening process, which degraded spectral information from the NIR band.

Figures 8 and 9 illustrate this decline – highlighting the necessity of optimizing pan-sharpening techniques when incorporating NIR data.

A feature-importance analysis (Figs. 10, 11) confirmed the negligible contribution of the NIR band toward classification and the justification for its exclusion for DS-4B.

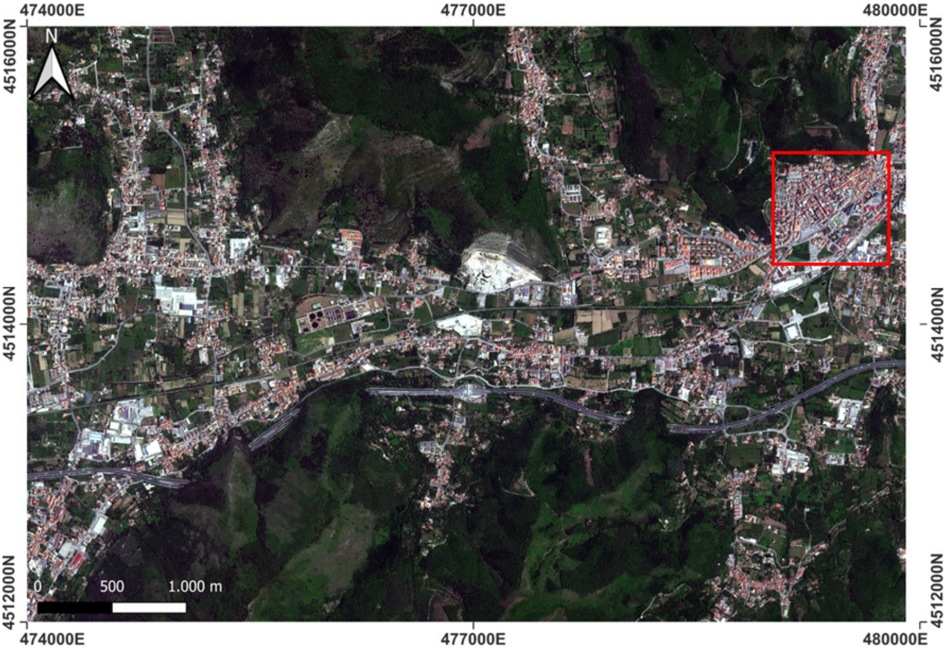

Fig. 6. Geolocation of zoomed-in location within study area (red rectangle)

Fig. 7. Zoom-in on small portion of study area to graphically show classification results for RGB composition (a) by following methods: SVM (b), DT (c), k-NN (d), NB (e), and RF (f)

Table 4. UA and PA results that were achieved by applying ML algorithms to DS-4B data set (highest value[s] for each class highlighted in bold)

Methods	Classes											
	Buildings		Road		Bare Soil		Tree Crop		Herbaceous Crop		Greenhouse	
	UA	PA	UA	PA	UA	PA	UA	PA	UA	PA	UA	PA
SVM	**0.99**	0.85	0.79	**0.97**	0.77	**0.90**	0.67	0.94	**0.92**	0.43	**0.99**	0.95
DT	0.90	0.85	**0.84**	0.90	0.83	0.85	**0.93**	0.89	0.85	0.92	**0.99**	0.93
NB	0.91	**0.91**	0.45	0.96	**0.91**	0.80	**0.92**	0.34	0.74	0.42	0.97	**0.97**
RF	0.94	0.87	0.87	**0.92**	0.76	0.88	0.65	**0.95**	0.86	0.36	**0.99**	0.93
k-NN	0.49	0.78	0.72	0.39	0.31	0.27	**0.93**	0.89	0.85	**0.91**	**0.99**	0.93

Table 5. CE and OE that were achieved by applying ML algorithms to DS-4B data set

Methods	Classes											
	Buildings		Roads		Bare Soil		Tree Crops		Herbaceous Crops		Greenhouses	
	CE	OE	CE	OE	CE	OE	CE	OE	CE	OE	CE	OE
SVM	0.01	0.15	0.21	0.03	0.23	0.10	0.33	0.06	0.08	0.57	0.01	0.05
DT	0.10	0.15	0.16	0.10	0.17	0.15	0.07	0.11	0.15	0.08	0.01	0.07
NB	0.09	0.09	0.55	0.04	0.09	0.20	0.08	0.66	0.26	0.58	0.03	0.03
RF	0.06	0.13	0.13	0.08	0.24	0.12	0.35	0.05	0.14	0.64	0.01	0.07
k-NN	0.51	0.22	0.28	0.61	0.69	0.73	0.07	0.11	0.15	0.09	0.01	0.07

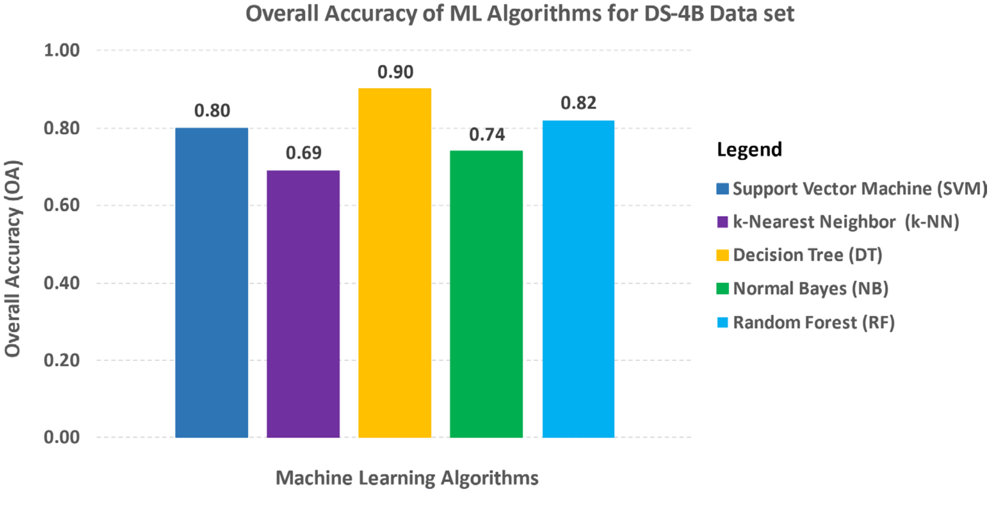

Fig. 8. OA levels that were achieved by different ML algorithms (SVM, k-NN, DT, NB, and RF) for DS-4B data set (colors represent respective algorithms as are indicated in legend)

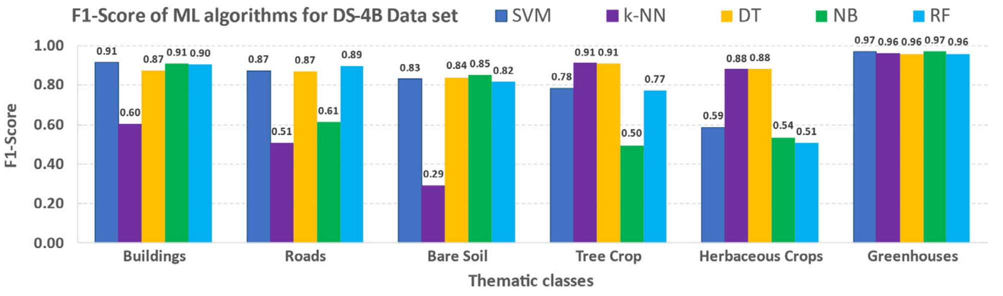

Fig. 9. F1-scores that were achieved by different ML algorithms (SVM, k-NN, DT, NB, and RF) for DS-4B data set (colors represent respective algorithms as are indicated in legend)

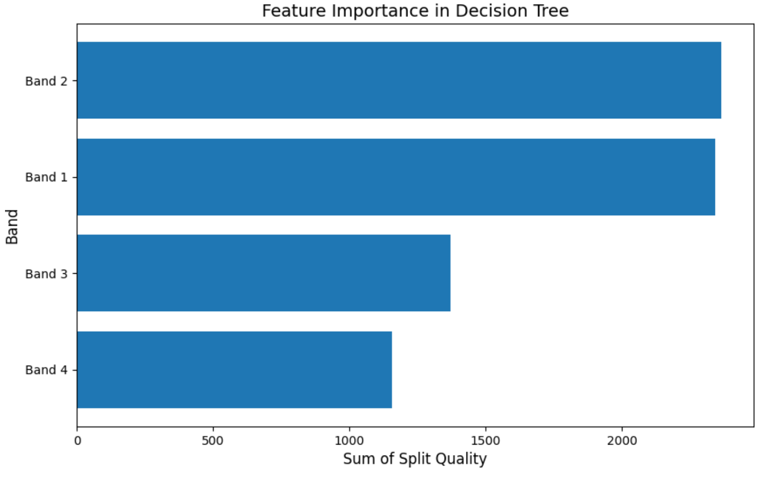

Fig. 10. Sum of split quality for each band in DT model

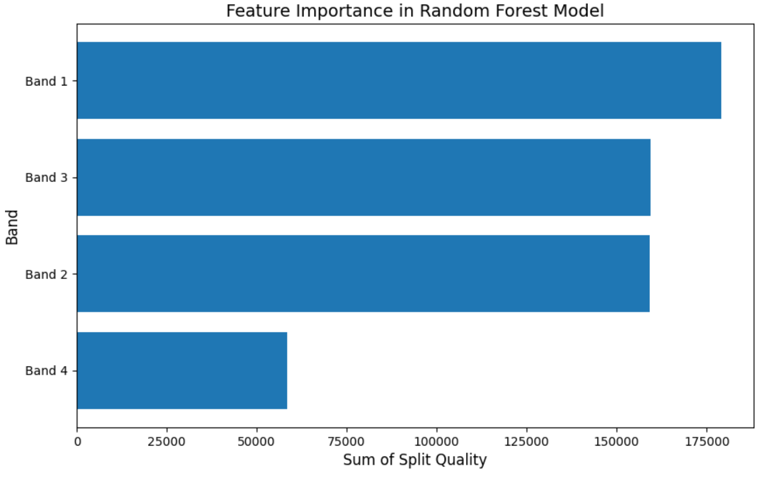

Fig. 11. Sum of split quality for each band in RF model

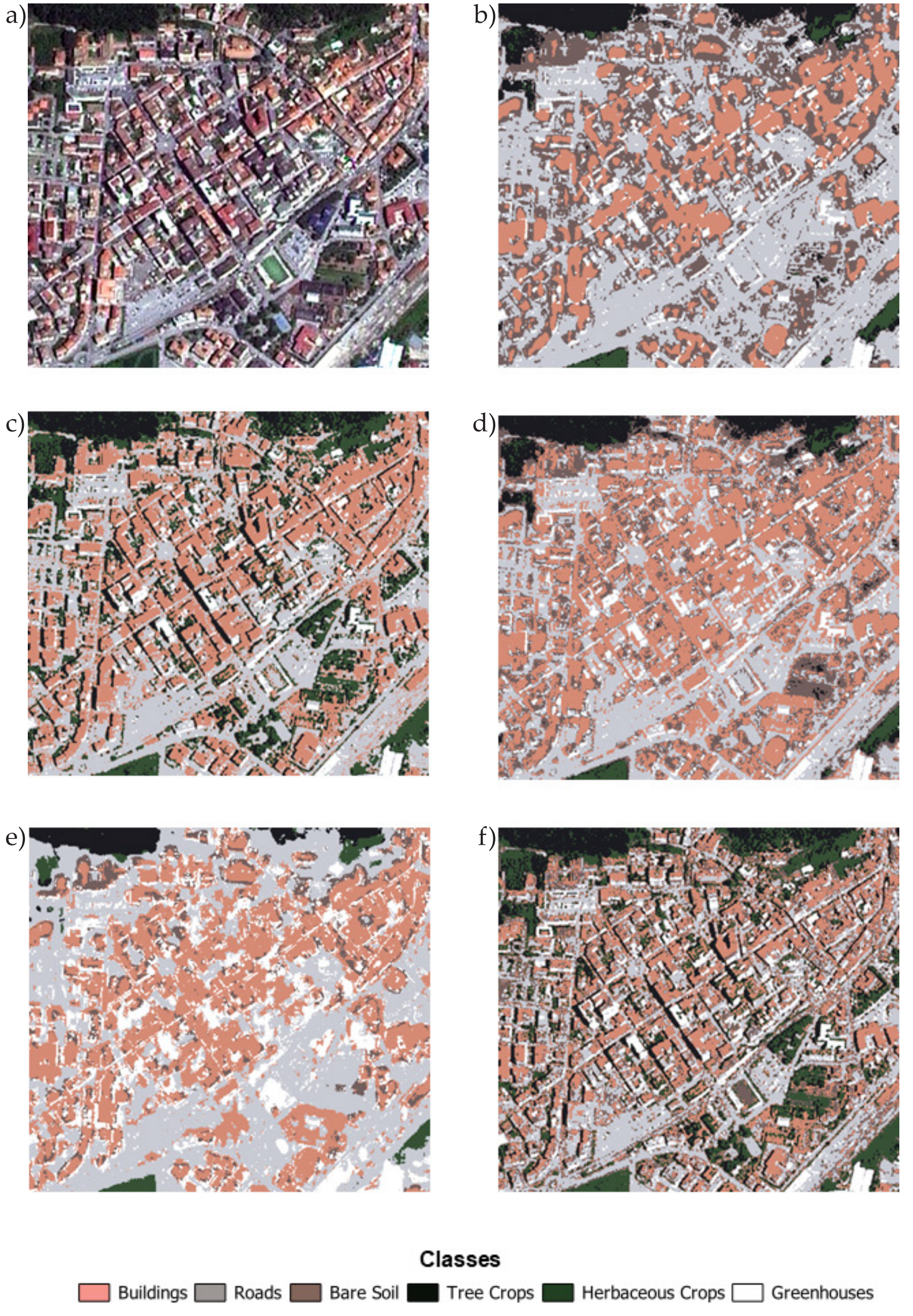

Fig. 12. Zoom-in on small portion of study area that graphically shows classification results for all multispectral band compositions when using following methods: RGB composition (a), SVM (b), DT (c), k-NN (d), NB (e), and RF (f)

The ability of DT to remove low-information features explains its superior performance relative to the other models when NIR bands are included. The findings demonstrated the value of spectral-band selection for remote-sensing classifications.

Figure 12 shows the thematic maps that were obtained from the classification of all of the multispectral bands for the same small portion of the study area that was considered previously.

Ultimately, the results indicated the most effective classifiers for DS-3B were k-NN and SVM, and the best for DS-4B was DT (since it could remove the non-informative spectral bands). As is evident from various research papers [67], no classifier in the field of machine learning has performed optimally in all scenarios. While some studies [68] have suggested that ANNs were more accurate than DTs, others [69] have suggested the opposite. While some findings [70, 71] have similarly suggested that the performances of SVM and R were equal in term of accuracy, others [72–75] have suggested that SVM was more accurate than RF. The reasons were generally the approach that was taken in each particular study.

A comparative study [76] that compared the performance of 30 data sets showed RF with the highest average accuracy (73.19%) – definitely better than SVM (62.28%); RF performed the best for just 18 out of the 30 data sets. The findings suggested that the role of each data set's characteristics determined the performance of each classifier and implied that no single algorithm could be considered to be universally superior.

The research also established the requirement for the appropriate choice of pan-sharpening methods and input spectral bands for the purpose of obtaining the best classification accuracy for high-resolution satellite data.

4. Conclusion

This study confirmed that machine-learning algorithms are effective for classifying high-resolution satellite images; however, the band composition of the imagery to be classified plays a fundamental role in producing accurate thematic maps.

In the classification of DS-4B (including the infrared band), SVM, k-NN, and NB yielded low UA and PA values for the herbaceous and tree crop classes (unlike when RGB composition was used). This issue may have stemmed from the pan-sharpening process, as the panchromatic channel did not include the near-infrared band. In fact, DT and RF were the only methods that were capable of achieving excellent results for the vegetation classification with DS-4B, as they automatically excluded the NIR band due to its low information gain during the attribute-selection process.

To improve the classification performance of multispectral pan-sharpened images, it is recommended that the panchromatic channel also include the infrared band – especially when vegetation is among the classes of interest. As demonstrated in this case study, classification results can be significantly affected and distorted by improperly pan-sharpened infrared data; this can lead to suboptimal PA and UA values and generate thematic maps that do not accurately reflect the ground conditions. The combined use of QGIS and OTB software enables the effective classification of high-resolution satellite images through supervised ML algorithms.

Funding

This research received no specific grant from any funding agency in the public, commercial, or not-for-profit sectors.

CRediT Author Contribution

D. M.: conducted bibliographic research, performed experiments using OTB in the GIS environment, conducted the accuracy tests, result analysis, and writing of the manuscript.

C. P.: conceived the article and designed the experiments, supervised the applications, managed the validation, result analysis, and writing of the manuscript.

S. F. B.: conceived the article and designed the experiments, conducted bibliographic research, organized the data collection, result analysis, and writing of the manuscript.

All authors have read and approved the final version of the paper.

Declaration of Competing Interests

The authors declare that they have no known competing financial interests or personal relationships that could have appeared to influence the work that was reported in this paper.

Use of Generative AI and AI-Assisted Technologies

No generative AI or AI-assisted technologies were employed in the preparation of this manuscript.

Acknowledgements

The authors would like to thank Carlo De Michele (CEO of Ariespace s.r.l.) for his availability and for providing the data that was essential for this research. His support has been fundamental during the development of this study.

References

[1] Papale D., Barbati A.: *Supporto informativo del telerilevamento per il monitoraggio e la valutazione funzionale dei rimboschimenti come mezzi di lotta alla desertificazione*. Geotema, vol. 25, 2005, pp. 31–37.

[2] Acharki S.: *PlanetScope contributions compared to Sentinel-2, and Landsat-8 for LULC mapping*. Remote Sensing Applications: Society and Environment, vol. 27, 2022, 100774. https://doi.org/10.1016/j.rsase.2022.100774.

[3] European Environment Agency (EEA): *E. CORINE Land Cover 2018 (Raster 100 m), Europe, 6-Yearly – Version 2020_20u1, May 2020*. 13.05.2020. https://doi.org/10.2909/960998c1-1870-4e82-8051-6485205ebbac.

[4] Diaz-Pacheco J., Gutiérrez J.: *Exploring the limitations of CORINE land cover for monitoring urban land-use dynamics in metropolitan areas.* Journal of Land Use Science, vol. 9(3), 2014, pp. 243–259. https://doi.org/10.1080/1747423X.2012.761736.

[5] Brown C.F., Brumby S.P., Guzder-Williams B., Birch T., Hyde S.B., Mazzariello J., Czerwinski W., Pasquarella V.J., Haertel R., Ilyushchenko S., Schwehr K., Weisse M., Stolle F., Hanson C., Guinan O., Moore R., Tait A.M.: *Dynamic World, Near real-time global 10 m land use land cover mapping.* Scientific Data, vol. 9(1), 2022, 251. https://doi.org/10.1038/s41597-022-01307-4.

[6] Venter Z.S., Barton D.N., Chakraborty T., Simensen T., Singh G.: *Global 10 m land use land cover datasets: A comparison of dynamic world, world cover and Esri land cover.* Remote Sensing, vol. 14(16), 2022, 4101. https://doi.org/10.3390/rs14164101.

[7] Giri C., Pengra B., Long J., Loveland T.R.: *Next generation of global land cover characterization, mapping, and monitoring.* International Journal of Applied Earth Observation and Geoinformation, vol. 25(1), 2013, pp. 30–37. https://doi.org/10.1016/j.jag.2013.03.005.

[8] Qin R., Liu T.: *A review of landcover classification with very-high resolution remotely sensed optical images – Analysis unit, model scalability and transferability.* Remote Sensing, vol. 14(3), 2022, 646. https://doi.org/10.3390/rs14030646.

[9] Rahman A., Abdullah H.M., Tanzir M.T., Hossain M.J. Khan B.M., Miah M.G., Islam I.: *Performance of different machine learning algorithms on satellite image classification in rural and urban setup.* Remote Sensing Applications: Society and Environment, vol. 20(5), 2020, 100410. https://doi.org/10.1016/j.rsase.2020.100410.

[10] Maxwell A.E., Warner T.A., Fang F.: *Implementation of machine-learning classification in remote sensing: An applied review*. International Journal of Remote Sensing, vol. 39(9), 2018, pp. 2784–2817. https://doi.org/10.1080/01431161.2018.1433343.

[11] Das S., Dey A., Pal A., Roy N.: *Applications of artificial intelligence in machine learning: Review and prospect*. International Journal of Computer Applications, vol. 115(9), 2015, pp. 31–41. https://doi.org/10.5120/20182-2402.

[12] Jordan M.I., Mitchell T.M.: *Machine learning: Trends, perspectives, and prospects*. Science, vol. 349(6245), 2015, pp. 255–260. https://doi.org/10.1126/science.aaa8415.

[13] Stilgoe J.: *Machine learning, social learning and the governance of self-driving cars.* Social Studies of Science, vol. 48(1), 2018, pp. 25–56. https://doi.org/10.1177/0306312717741687.

[14] Karpatne A., Ebert-Uphoff I., Ravela S., Babaie H.A., Kumar V.: *Machine learning for the geosciences: Challenges and opportunities*. IEEE Transactions on Knowledge and Data Engineering, vol. 31(8), 2018, pp. 1544–1554. https://doi.org/10.1109/TKDE.2018.2861006.

[15] Ziadia A., Habibi M., Kelouwani S.: *Machine learning study of the effect of process parameters on tensile strength of FFF PLA and PLA-CF*. Eng, vol. 4(4), 2023, pp. 2741–2763. https://doi.org/10.3390/eng4040156.

[16] Caruana R., Niculescu-Mizil A.: *An empirical comparison of supervised learning algorithms*, [in:] *ICML '06: Proceedings of the 23rd International Conference on Machine Learning,* Association for Computing Machinery, New York, pp. 161–168. https://doi.org/10.1145/1143844.1143865.

[17] Campbell C., Ying Y.: *Support Vector Machines for Classification*, [in:] Campbell C., Ying Y., *Learning with Support Vector Machines*, Synthesis Lectures on Artificial Intelligence and Machine Learning, Springer, Cham, Switzerland 2022, pp. 1–25.

[18] Pires de Lima R., Marfurt K.: *Convolutional neural network for remote-sensing scene classification: Transfer learning analysis*. Remote Sensing, vol. 12(1), 2019, 86. https://doi.org/10.3390/rs12010086.

[19] Perlich C., Provost F., Simonoff J.: *Tree induction vs. logistic regression: A learning-curve analysis*. Journal of Machine Learning Research, vol. 4, 2003, pp. 211–255.

[20] Tariq A., Jiango Y., Li Q., Gao J., Lu L., Soufan W., Almutairi K.F., Habibur-Rahman M.: *Modelling, mapping and monitoring of forest cover changes, using support vector machine, Kernel logistic regression and naive Bayes tree models with optical remote sensing data*. Heliyon, vol. 9(2), 2023, e13212. https://doi.org/10.1016/j.heliyon.2023.e13212.

[21] Belgiu M., Drăguţ L.: *Random Forest in remote sensing: A review of applications and future directions.* ISPRS Journal of Photogrammetry and Remote Sensing, vol. 114, 2016, pp. 24–31. https://doi.org/10.1016/j.isprsjprs.2016.01.011.

[22] Xu M., Watanachaturaporn P., Varshney P.K., Arora M.K.: *Decision tree regression for soft classification of remote sensing data.* Remote Sensing of Environment, vol. 97(3), 2005, pp. 322–336. https://doi.org/10.1016/j.rse.2005.05.008.

[23] Blanzieri E., Melgani F.: *Nearest neighbor classification of remote sensing images with the maximal margin principle*. IEEE Transactions on Geoscience and Remote Sensing, vol. 46(6), 2008, pp. 1804–1811. https://doi.org/10.1109/TGRS.2008.916090.

[24] Dash S.S., Nayak S.K., Mishra D.: *A review on machine learning algorithms*, [in:] Mishra D., Buyya R., Mohapatra P., Patnaik S. (eds.), *Intelligent and Cloud Computing: Proceedings of ICICC 2019, Volume 2*, Smart Innovation, Systems and Technologies, vol. 153, Springer, Singapore 2020, pp. 495–507. https://doi.org/10.1007/978-981-15-6202-0_51.

[25] Kassambara A.: *Practical Guide to Cluster Analysis in R: Unsupervised Machine Learning.* STHDA, Marseille 2017.

[26] Alloghani M., Al-Jumeily D., Mustafina J., Hussain A., Aljaaf A.J.: *A systematic review on supervised and unsupervised machine learning algorithms for data science*, [in:] Berry M.W., Mohamed A., Bee W.Y. (eds.), *Supervised and Unsupervised Learning for Data Science*, Springer, Cham 2020, pp. 3–21. https://doi.org/10.1007/978-3-030-22475-2_1.

[27] Abbas A.W., Minallh N., Ahmad N., Abid S.A.R., Khan M.A.A.: *K-Means and ISODATA clustering algorithms for landcover classification using remote sensing*. Sindh University Research Journal (Science Series), vol. 48(2), 2016, pp. 315–318.

[28] European Space Agency (ESA). https://earth.esa.int/eogateway/missions/spot-7 [access: 8.12.2024].

[29] National Aeronautics and Space Administration (NASA): *Landsat Orbit Swath*. https://svs.gsfc.nasa.gov/11481 [access: 26.01.2025].

[30] Ehlers M., Klonus S., Johan Åstrand P., Rosso P.: *Multi-sensor image fusion for pansharpening in remote sensing.* International Journal of Image and Data Fusion, vol. 1(1), 2010, pp. 25–45. https://doi.org/10.1080/19479830903561985.

[31] Alcaras E., Parente C.: *The effectiveness of pan-sharpening algorithms on different land cover types in GeoEye-1 satellite images*. Journal of Imaging, vol. 9(5), 2023, 93. https://doi.org/10.3390/jimaging9050093.

[32] Gupta D.K., Prashar S., Singh S., Srivastava P.K., Prasad R.: *Introduction to RADAR remote sensing*, [in:] Srivastava P.K., Gupta D.K., Islam T., Han D., Prasad R. (eds.), *Radar Remote Sensing: Applications and Challenges*, Elsevier, 2022, pp. 3–27. https://doi.org/10.1016/B978-0-12-823457-0.00018-5.

[33] Vapnik V.: *The Nature of Statistical Learning Theory*. Springer Science & Business Media, New York 1999. https://doi.org/10.1007/978-1-4757-3264-1.

[34] Pal M., Mather P.M.: *Support vector machines for classification in remote sensing*. International Journal of Remote Sensing, vol. 26(5), 2005, pp. 1007–1011. https://doi.org/10.1080/01431160512331314083.

[35] Amarappa S., Sathyanarayana S.V.: *Data classification using Support Vector Machine (SVM), a simplified approach*. International Journal of Electronics and Computer Science Engineering, vol. 3(4), 2014, pp. 435–445.

[36] Melgani F., Bruzzone L.: *Classification of hyperspectral remote sensing images with support vector machines.* IEEE Transactions on Geoscience and Remote Sensing, vol. 42(8), 2004, pp. 1778–1790. https://doi.org/10.1109/TGRS.2004.831865.

[37] Shan F., He X., Xu H., Armaghani D.J., Sheng D.: *Applications of machine learning in mechanised tunnel construction: A systematic review*. Eng, vol. 4(2), 2023, pp. 1516–1535. https://doi.org/10.3390/eng4020087.

[38] Wang M., Wan Y., Ye Z., Lai X.: *Remote sensing image classification based on the optimal support vector machine and modified binary coded ant colony optimization algorithm*. Information Sciences, vol. 402, 2017, pp. 50–68. https://doi.org/10.1016/j.ins.2017.03.027.

[39] Foody G.M., Mathur A.: *A relative evaluation of multiclass image classification by support vector machines.* IEEE Transactions on Geoscience and Remote Sensing, vol. 42(6), 2004, pp. 1335–1343. https://doi.org/10.1109/TGRS.2004.827257.

[40] Pal M., Foody G.M.: *Evaluation of SVM, RVM and SMLR for accurate image classification with limited ground data*. IEEE Journal of Selected Topics in Applied Earth Observations and Remote Sensing, vol. 5(5), 2012, pp. 1344–1355. https://doi.org/10.1109/JSTARS.2012.2215310.

[41] Pal M., Mather P.M.: *An assessment of the effectiveness of decision tree methods for land cover classification*. Remote Sensing of Environment, vol. 86(4), 2003, pp. 554–565. https://doi.org/10.1016/S0034-4257(03)00132-9.

[42] Amoroso P.P., Ciaramella A., Ferone A., Parente C., Staiano A.: *Application of decision tree algorithm on Landsat 9 OLI-2 images for coastline extraction*, [in:] *2024 IEEE International Workshop on Metrology for the Sea: Learning to Measure Sea Health Parameters (MetroSea)*, IEEE, pp. 358–363. https://doi.org/10.1109/MetroSea62823.2024.10765729.

[43] Suthaharan S.: *Decision tree learning*, [in]: Suthaharan S., *Machine Learning Models and Algorithms for Big Data Classification: Thinking with Examples for Effective Learning*, Integrated Series in Information Systems, vol. 36, Springer, Boston 2016, pp. 237–269. https://doi.org/10.1007/978-1-4899-7641-3_10.

[44] Pal M., Mather P.M.: *Decision tree-based classification of remotely sensed data*, [in:] *Proceedings of the 22nd Asian Conference on Remote Sensing: 5–9 November, 2001, Singapore. Volume 5*, Center for Remote Imaging, Sensing and Processing, National University of Singapore, Queenstown 2001, p. 9.

[45] Berhane T.M., Lane C.R., Wu Q., Autrey B.C., Anenkhonov O.A., Chepinoga V.V., Liu, H.: *Decision-tree, rule-based, and random forest classification of high-resolution multispectral imagery for wetland mapping and inventory*. Remote Sensing, vol. 10(4), 2018, 580. https://doi.org/10.3390/rs10040580.

[46] Friedl M.A., Brodley C.E.: *Decision tree classification of land cover from remotely sensed data.* Remote Sensing of Environment, vol. 61(3), 1997, pp. 399–409. https://doi.org/10.1016/S0034-4257(97)00049-7.

[47] Fukunaga K.: *Introduction to Statistical Pattern Recognition.* Academic Press, New York 1990.

[48] Open Computer Vision: *Normal Bayes Classifier*. https://docs.opencv.org/2.4/modules/ml/doc/normal_bayes_classifier.html [access: 8.12.2024].

[49] Ahmad A., Sakidin H., Sari M.Y.A., Sufahani S.F.: *Naïve Bayes classification of high-resolution aerial imagery.* International Journal of Advanced Computer Science and Applications, vol. 12(11), 2021, pp. 168–177. https://doi.org/10.14569/IJACSA.2021.0121120.

[50] Solares C., Sanz A.M.: *Different Bayesian network models in the classification of remote sensing images*, [in:] Yin H., Tino P., Corchado E., Byrne W., Yao X. (eds.), *Intelligent Data Engineering and Automated Learning – IDEAL 2007: 8th International Conference, Birmingham, UK, December 16–19, 2007: Proceedings*, Lecture

Notes in Computer Science, vol. 4881, Springer, Berlin, Heidelberg 2007, pp. 10–16. https://doi.org/10.1007/978-3-540-77226-2_2.

[51] Yang B., Yu X.: *Remote sensing image classification of geoeye-1 high-resolution satellite.* The International Archives of the Photogrammetry, Remote Sensing and Spatial Information Sciences, vol. XL-4, 2014, pp. 325–328. https://doi.org/10.5194/isprsarchives-XL-4-325-2014.

[52] Chao L.I., Wen-Hui Z., Ran L.I., Jun-Yi W., Ji-Ming L.: *Research on star/galaxy classification based on stacking ensemble learning.* Chinese Astronomy and Astrophysics, vol. 44(3), 2020, pp. 345–355. https://doi.org/10.1016/j.chinastron.2020.08.005.

[53] Breiman L.: *Random forests*. Machine Learning, vol. 45(1), 2001, pp. 5–32. https://doi.org/10.1023/A:1010933404324.

[54] Levatić J., Ceci M., Kocev D., Džeroski S.: *Semi-supervised classification trees.* Journal of Intelligent Information Systems, vol. 49(3), 2017, pp. 461–486. https://doi.org/10.1007/s10844-017-0457-4.

[55] Waske B., Benediktsson J.A., Sveinsson J.R.: *Random Forest Classification of Remote Sensing Data*, [in:] Chen C.H. (ed.), *Signal and Image Processing for Remote Sensing*, CRC Press, Boca Raton 2012, pp. 365–374.

[56] Gislason P.O., Benediktsson J.A., Sveinsson J.R.: *Random Forest classification of multisource remote sensing and geographic data*, [in:] *IGARSS 2004: 2004 IEEE International Geoscience and Remote Sensing Symposium. Volume 2*, IEEE, 2004, pp. 1049–1052. https://doi.org/10.1109/IGARSS.2004.1368591.

[57] Akar Ö., Güngör O.: *Classification of multispectral images using Random Forest algorithm.* Journal of Geodesy and Geoinformation, vol. 1(2), 2012, pp. 105–112. https://doi.org/10.9733/jgg.241212.1.

[58] McRoberts R.E., Nelson M.D., Wendt D.G.: *Stratified estimation of forest area using satellite imagery, inventory data, and the k-Nearest Neighbors technique.* Remote Sensing of Environment, vol. 82(2–3), 2002, pp. 457–468. https://doi.org/10.1016/S0034-4257(02)00064-0.

[59] Nurwauziyah I., Umroh Dian S., Putra I.G.B., Firdaus M.I.: *Satellite image classification using Decision Tree, SVM and k-Nearest Neighbor.* Department of Geomatics, National Cheng Kung University, Tainan, Taiwan, July 2018.

[60] Alcaras E., Amoroso P.P., Figliomeni F.G., Parente C., Vallario A.: *Machine learning approaches for coastline extraction from Sentinel-2 images: K-Means and K-Nearest Neighbour algorithms in comparison*, [in:] Borgogno-Mondino E., Zamperlin P. (eds.), *Geomatics for Green and Digital Transition: 25th Italian Conference, ASITA 2022, Genova, Italy, June 20–24, 2022: Proceedings*, Communications in Computer and Information Science, vol. 1651, Springer, Cham 2022, pp. 368–379. https://doi.org/10.1007/978-3-031-17439-1_27.

[61] Triguero I., García-Gil D., Maillo J., Luengo J., García S., Herrera F.: *Transforming big data into smart data: An insight on the use of the k-nearest neighbors algorithm to obtain quality data.* Wiley Interdisciplinary Reviews: Data Mining and Knowledge Discovery, vol. 9(2), 2019, e.1289. https://doi.org/10.1002/widm.1289.

[62] Thanh Noi P., Kappas M.: *Comparison of random forest, k-nearest neighbor, and support vector machine classifiers for land cover classification using Sentinel-2 imagery.* Sensors, vol. 18(1), 2017, 18. https://doi.org/10.3390/s18010018.

[63] Abedi R., Bonyad A.E.: *Estimation and mapping forest attributes using "k nearest neighbor" method on IRS-P6 LISS III satellite image data.* Ecologia Balkanica, vol. 7(1), 2015, pp. 93–102.

[64] Strahler A.H., Boschetti L., Foody G.M., Friedl M.A., Hansen M.C., Herold M., Mayaux P., Morisette J.T., Stehman S.V., Woodcock C.E.: *Global Land Cover Validation: Recommendations for Evaluation and Accuracy Assessment of Global Land Cover Maps.* European Communities, Luxembourg 2006.

[65] Foody G.M.: *Thematic map comparison: Evaluating the statistical significance of differences in classification accuracy.* Photogrammetric Engineering & Remote Sensing, vol. 70(5), 2004, pp. 627–633. https://doi.org/10.14358/PERS.70.5.627.

[66] Fung T., LeDrew E.: *The determination of optimal threshold levels for change detection using various accuracy*. Photogrammetric Engineering and Remote Sensing, vol. 54(10), 1988, pp. 1449–1454.

[67] Lawrence R.L., Moran C.J.: *The AmericaView classification methods accuracy comparison project: A rigorous approach for model selection.* Remote Sensing of Environment, vol. 170, 2015, pp. 115–120. https://doi.org/10.1016/j.rse.2015.09.008.

[68] Rogan J., Franklin J., Stow D., Miller J., Woodcock C., Roberts D.: *Mapping land-cover modifications over large areas: A comparison of machine learning algorithms.* Remote Sensing of Environment, vol. 112(5), 2008, pp. 2272–2283. https://doi.org/10.1016/j.rse.2007.10.004.

[69] Lippitt C.D., Rogan J., Li Z., Eastman J.R., Jones T.G.: *Mapping selective logging in mixed deciduous forest.* Photogrammetric Engineering & Remote Sensing, vol. 74(10), 2008, pp. 1201–1211. https://doi.org/10.14358/PERS.74.10.1201.

[70] Pal M.: *Random forest classifier for remote sensing classification.* International Journal of Remote Sensing, vol. 26(1), 2005, pp. 217–222. https://doi.org/10.1080/01431160412331269698.

[71] Adam E., Mutanga O., Odindi J., Abdel-Rahman E.M.: *Land-use/cover classification in a heterogeneous coastal landscape using RapidEye imagery: evaluating the performance of random forest and support vector machines classifiers.* International Journal of Remote Sensing, vol. 35(10), 2014, pp. 3440–3458. https://doi.org/10.1080/01431161.2014.903435.

[72] Zhang C., Xie Z.: *Object-based vegetation mapping in the Kissimmee River watershed using HyMap data and machine learning techniques.* Wetlands, vol. 33(2), 2013, pp. 233–244. https://doi.org/10.1007/s13157-012-0373-x.

[73] Maxwell A.E., Strager M.P., Warner T.A., Zégre N.P., Yuill C.B.: *Comparison of NAIP orthophotography and RapidEye satellite imagery for mapping of mining and mine reclamation.* GIScience & Remote Sensing, vol. 51(3), 2014, pp. 301–320. https://doi.org/10.1080/15481603.2014.912874.

[74] Maxwell A.E., Warner T.A., Strager M.P., Pal M.: *Combining RapidEye satellite imagery and Lidar for mapping of mining and mine reclamation.* Photogrammetric Engineering & Remote Sensing, vol. 80(2), 2014, pp. 179–189. https://doi.org/10.14358/PERS.80.2.179-189.

[75] Maxwell A.E., Warner T.A., Strager M.P., Conley J.F., Sharp A.L.: *Assessing machine-learning algorithms and image-and lidar-derived variables for GEOBIA classification of mining and mine reclamation.* International Journal of Remote Sensing, vol. 36(4), 2015, pp. 954–978. https://doi.org/10.1080/01431161.2014.1001086.

[76] Ibrahim S.A.: *Improving land use/cover classification accuracy from random forest feature importance selection based on synergistic use of sentinel data and digital elevation model in agriculturally dominated landscape*. Agriculture, vol. 13(1), 2022, 98. https://doi.org/10.3390/agriculture13010098.